

Motions in the Interiors and Atmospheres of Jupiter and Saturn

2. Barotropic Instabilities and Normal Modes of an Adiabatic Planet¹

ANDREW P. INGERSOLL AND RONALD L. MILLER²

*Division of Geological and Planetary Sciences, California Institute of Technology,
Pasadena, California 91125*

Received June 3, 1985; revised September 30, 1985

The low-frequency motions in a rotating, adiabatic, inviscid fluid planet are barotropic, quasi-geostrophic, and quasi-columnar. The only steady motions are differentially rotating cylinders in which zonal velocity \bar{u} is a function of cylindrical radius r . Projected onto the planetary surface the limiting curvature at which the flow becomes unstable is negative; its amplitude is three to four times the amplitude for thin atmospheres, for planets in which density decreases linearly to zero at the surface. This result, derived first by A. P. Ingersoll and D. Pollard (1982, *Icarus* 52, 62–80) for low zonal wavenumber perturbations, is shown to hold for all quasi-columnar perturbations. When $\bar{u} = 0$ the small amplitude motions are oscillatory. The lowest mode, as regards structure parallel to the axis, propagates eastward with a speed proportional to (wavelength)². Both the barotropic stability criterion and the phase speed of the normal mode oscillations have features in common with Jupiter and Saturn observations, although the test is inconclusive with current data and theory. © 1986 Academic Press, Inc.

INTRODUCTION

This is the second paper in a series dealing with possible large-scale motions in the giant planets' fluid interiors. The first paper (Ingersoll and Pollard, 1982, hereinafter referred to as IP) presented a scale analysis and a set of equations describing motions in a rotating sphere of variable density when the eddy viscosity and superadiabaticity are small. A simple problem was solved, that of an inviscid adiabatic fluid sphere with a steady zonal wind varying as a function of cylindrical radius. This differentially rotating, concentric cylinder pattern was known to be a possible steady-state configuration (Poincare, 1910), but its hydrodynamic stability had not been previously in-

vestigated. IP restricted their analysis to perturbations of low zonal wavenumber, and found that stability is controlled by a parameter B analogous to β , the parameter which enters in the barotropic stability criterion for thin atmospheric layers (e.g., Holton, 1979). The two parameters differ in both sign and magnitude, however, so the barotropic stability criterion for deep fluid spheres is significantly different from that for thin layers. IP concluded that Jupiter's and Saturn's observed zonal wind profiles are close to marginal stability according to this deep sphere criterion, but are several times supercritical according to the thin atmosphere criterion.

The present paper extends the analysis of IP to a more general class of flows. If the zonal jet spacing L is much less than the planetary radius a_0 the fastest growing perturbations have zonal wavenumbers of order a_0/L , which is large. These perturbations are outside the class considered by IP. The motion is then quasi-columnar in that the scale of variation in a plane perpendicu-

¹ Contribution Number 4217 of the Division of Geological and Planetary Sciences, California Institute of Technology, Pasadena, Calif. 91125.

² Current address: Department of Earth, Atmospheric, and Planetary Sciences, Center for Meteorology and Physical Oceanography, Massachusetts Institute of Technology, Cambridge, Mass. 02139.

lar to the axis of rotation is much less than the scale parallel to the axis. The resulting equations are nonseparable, and the mathematical difficulties are greater than those faced by IP.

Below we examine the stability of the rotating cylinder flow to the more general class of perturbations. We solve for the growth rates and spatial structure of the perturbations. The stability criterion is once again a condition on the curvature of the zonal velocity profile, and we compare these new results with those obtained by IP and with Voyager observations. The mathematical method is also used to study the low-frequency modes of oscillation of a rotating adiabatic fluid sphere. A comparison is made between these modes and ordinary Rossby waves in a thin atmosphere as well as waves on Jupiter.

The motivation for this study is twofold. First, these low-frequency, inviscid, adiabatic, quasi-columnar motions represent a new example of geostrophic flow, and deserve study for their own sake. Second, the internal motions of Jupiter and Saturn probably affect the flow in the visible atmospheres. Certain features of the observed circulation—the curvature of the zonal velocity profile (IP), the preponderance of strong eastward flow on Saturn (Smith *et al.*, 1982; IP), the existence and time-dependent behavior of long-lived ovals (Ingersoll and Cuong, 1981; Mac Low and Ingersoll, 1985)—may be inconsistent with some of the hypotheses about internal motions or lack thereof. Thus, surface observations may tell us something about the interior. But first we must find out what kinds of internal flows are possible, that is, consistent with the equations of motion. The present paper is a step toward that goal. For a general review of atmospheric dynamics of Jupiter and Saturn the reader is referred to Ingersoll *et al.* (1984).

MATHEMATICAL MODEL

IP derived the anelastic equations of motion (Ogura and Phillips, 1962) that describe

slow motions in a rotating, quasi-adiabatic fluid sphere. These equations are self-consistent in that they conserve energy. Their advantage is that they do not propagate sound waves. IP further restricted consideration to the case of an adiabatic fluid—one where entropy per unit mass is constant both with respect to time and position. These equations, IP (40) and (46), describe the quasi-columnar motions of a rotating barotropic fluid. The motion takes place in a cylindrical annulus of radius $r \sim r_0 = a_0 \cos \lambda$, where λ is the latitude at which the cylinder meets the surface of the planet. The radial thickness of the annulus is of order L , and the condition $L \ll a_0$ allows us to unwrap the annulus and treat it using Cartesian coordinates. The spherical geometry still enters in the density structure and in the boundary condition which states that the normal component of velocity is zero at the planetary surface. The coordinate system and choice of length scales are reviewed in the Appendix.

Any zonal flow \bar{u} that depends only on cylindrical radius r is a steady solution. IP derive the linear equations that govern small amplitude perturbations superposed on this basic zonal flow. These equations, IP (48)–(53), are the starting point of our analysis:

$$u = \bar{u} - \frac{\partial \phi}{\partial y} \exp[ik(x - ct)], \quad (1)$$

$$v = ik\phi \exp[ik(x - ct)], \quad (2)$$

$$w = ik\mathbf{w} \exp[ik(x - ct)], \quad (3)$$

$$(\bar{u} - c) \left(\frac{\partial^2 \phi}{\partial y^2} - k^2 \phi \right) + \left(\frac{b}{\rho} \frac{\partial \rho}{\partial r} - \frac{d^2 \bar{u}}{dy^2} \right) \phi = \frac{b}{\rho} \frac{\partial(\rho \mathbf{w})}{\partial z}, \quad (4)$$

$$(\bar{u} - c)k^2 \mathbf{w} = b \frac{\partial \phi}{\partial z}, \quad (5)$$

$$\rho \mathbf{w} = \pm \rho \phi \cot \lambda,$$

$$z = \pm h = \pm \sin \lambda. \quad (6)$$

Here (x, y, z) are Cartesian coordinates with x to the east, y inward along a cylindri-

cal radius, and z parallel to the axis of rotation. The dependent variables ϕ and \mathbf{w} are assumed to vary on a scale L in the y direction and on a scale comparable to the planetary radius in the z direction. Departing slightly from IP we scale r and z by the planetary radius a_0 rather than the cylindrical radius $a_0 \cos \lambda$. The velocities corresponding to (x, y, z) are (u, v, w) . The unperturbed zonal flow is $\bar{u}(y)$, and it is scaled by a velocity u_0 . The wavenumber k and eastward phase speed c of the disturbance are scaled by L^{-1} and u_0 , respectively. Time t is scaled by L/u_0 . Although the above equations are dimensionless, we will frequently include scaling factors in our formulas to clarify the physical dependence.

The important dimensionless numbers are b^{-1} and δ , where

$$b^{-1} = u_0 a_0 / (2\Omega L^2) = O(1), \tag{7}$$

$$\delta = L/a_0 \ll 1. \tag{8}$$

The fact that the aspect ratio δ and the Rossby number $\varepsilon = b^{-1}\delta$ are small justifies the quasi-geostrophic approximation for this problem. Since density ρ varies on the scale of the planetary radius but not on the scale of L , both ρ , $(1/\rho)\partial\rho/\partial r$ and $(1/\rho)\partial\rho/\partial z$ are of order unity and vary smoothly in z . Their y variation is negligible for disturbances of scale $L \ll a_0$. Generally we use a polytropic model of the density

$$\rho(R) = \rho_0 \frac{\sin(\pi R)}{(\pi R)}, \quad R = (r^2 + z^2)^{1/2}. \tag{9}$$

Here R is the dimensionless spherical radius, with $R = 1$ at the planetary surface; r is the dimensionless cylindrical radius, with $r = r_0 = a_0 \cos \lambda$ in the middle of the annulus.

To examine the stability of a particular zonal flow $\bar{u}(y)$ we solve Eqs. (4) and (5) for the eigenvalue c . The equations are linear partial differential equations in the variables $\phi(y, z)$ and $\mathbf{w}(y, z)$. The eigenvalue is $c = c_r + ic_i$, so c_r is the phase speed and kc_i is the growth rate of the disturbance. Most

of the examples are for the profile

$$\bar{u} = u_0 \cos(\pi y/L), \quad |y| \leq L, \tag{10}$$

which is a single cosine jet with peak eastward velocity in the middle of the channel. (One may either regard y and L as physical quantities, or else take $L = 1$ and treat y as dimensionless.) A few comparisons are made with double and quadruple cosine jets—the same profile as in (10) but for the regions $-L \leq y \leq 3L$ and $-L \leq y \leq 7L$. An increase in the parameter b^{-1} corresponds to an increase in the curvature of the velocity profile. For any given b^{-1} the problem is to vary the disturbance wavenumber k to find whether the given profile is unstable; that is, whether positive values of kc_i exist.

For this barotropic flow model, growing disturbances get their energy from the kinetic energy of the zonal flow. This requirement is seen by considering the equation for disturbance kinetic energy:

$$\begin{aligned} \frac{1}{2} kc_i \int \int \left(\left| \frac{\partial \phi}{\partial y} \right|^2 + k^2 |\phi|^2 \right. \\ \left. + k^2 |\mathbf{w}|^2 \right) \rho dy dz = \frac{1}{2} \int \int \frac{d\bar{u}}{dy} \\ \text{Im} \left(k \phi^* \frac{\partial \phi}{\partial y} \right) \rho dy dz. \end{aligned} \tag{11}$$

To derive this equation, multiply Eq. (4) by $\rho \phi^*$, multiply Eq. (5)* by $\rho \mathbf{w}$, add the two equations, integrate over the domain, and take the imaginary part of the result. Here an asterisk denotes the complex conjugate. Both the $\partial^2 \phi / \partial y^2$ term and the $\partial(\rho \mathbf{w}) / \partial z$ term in (4) are integrated once by parts. The surface terms arising from the integrations by parts are assumed to vanish.

The lateral surface term is proportional to $\rho \phi^* \partial \phi / \partial y$, which vanishes if we impose the boundary condition

$$\phi = 0, \quad y = \pm L. \tag{12}$$

This condition is equivalent to having solid walls on the sides of the channel. One way to show that these artificial boundaries do not affect the calculation is to vary their position, for example, by comparing the

single and double jet solutions with each other. The other surface term has the form

$$b\rho\phi^*\mathbf{w} = \pm b\rho|\phi|^2 \cot \lambda, \quad z = \pm \sin \lambda, \quad (13)$$

where we have used the boundary condition (6). The fact that this term has no imaginary part means that this term also does not contribute to the energy balance. The energy equation (11) is obtained after multiplying the result of these manipulations by $k/2$.

From Eqs. (1)–(3) it follows that the left side of (11) is $d\bar{K}/dt$, the rate of change of disturbance kinetic energy. The factor 1/2 is needed because, although disturbance energy grows at the rate $2kc_i$, there is a factor of 1/2 in the expression for kinetic energy and another factor of 1/2 from averaging over cycles in x . The right side of (11) can be rewritten so that the equation becomes

$$\frac{d\bar{K}}{dt} = - \int \int \frac{d\bar{u}}{dy} \overline{u'v'} p dy dz, \quad (14)$$

where u' and v' are the disturbance velocity components in the x and y directions, and the overbar denotes an average over cycles in x .

The right side of (14) is thus the sole source of disturbance kinetic energy for this barotropic flow model. For the disturbance to grow the term $\overline{u'v'}$ must be positive where $d\bar{u}/dy$ is negative and vice versa; the disturbance must transfer x momentum out of the center of the jet. This is opposite to the transfer that was actually observed by Ingersoll *et al.* (1981) in Jupiter's atmosphere, indicating that the observed eddies on average are different from those considered here. Our result may still be relevant to Jupiter and Saturn if at deeper levels the curvature of the zonal velocity profile is limited by these unstable barotropic eddies. Ultimately the relevance of this barotropic model depends on the interior being adiabatic, as stated at the outset.

We shall also study the solutions obtained by setting $\bar{u} = 0$ in Eqs. (4) and (5).

From (11) it follows that $c_i = 0$; these solutions are wavelike in character and do not grow in time. The velocity scale u_0 is now arbitrary, but by setting $b = \cos \lambda$ in (7) we adopt the velocity scale $2\Omega L^2/r_0$, where L is the length scale of the disturbance and $r_0 = a_0 \cos \lambda$ is the cylindrical radius in physical units. The phase speed will therefore be given in terms of $2\Omega L^2/r_0$. With $\bar{u} = 0$ the coefficients multiplying the terms in ϕ and \mathbf{w} do not depend on y over the distance of L . Therefore the y dependence may be factored out, and the disturbance has the form

$$f(z) \exp[ik(x - ct) + iny]. \quad (15)$$

The problem is to find the eigensolutions $f(z)$ and the real eigenvalue c for different choices of k and n . The phase speed $c(k, n)$ may be compared to the phase speeds of waves in thin atmospheric layers and waves observed on Jupiter and Saturn.

METHOD OF SOLUTION

IP considered the case $k \rightarrow 0$, which means that the physical wavenumber of the disturbance is much less than L^{-1} , where L is the width of the jet (10). In this case Eq. (5) becomes $\partial\phi/\partial z = 0$, and (4) may be integrated with respect to z to yield a differential equation in y only. Below we do not restrict the value of k , so the differential equations (4) and (5) are not separable in y and z . Galerkin methods are used to find the solution (e.g., Haltiner and Williams, 1980).

We represent the solution as a sum of basis functions

$$\phi = \sum_{j=1}^J \sum_{m=1}^M \phi_{jm} f_j(z) g_m(y), \quad (16)$$

and similarly for \mathbf{w} . Here ϕ_{jm} are the unknown coefficients, and $f_j g_m$ are the chosen basis functions. For the z direction we use a finite element decomposition with $f_j(z)$ being piecewise linear functions centered on $J + 1$ equally spaced nodes in the range $|z| \leq \sin \lambda$. The reader is referred to Haltiner and Williams for details. The number of finite elements, or intervals, from $z = -\sin \lambda$ to z

$= \sin \lambda$ is J , and $J/2$ is the number of elements from the equator at $z = 0$ to the surface at $z = \sin \lambda$. Accordingly, $J = 2$ has a node at the equator and a node at the surface, and is called the 1-element model; $J = 4$ has an additional node halfway between the surface and the equator and is called the 2-element model, and so on. We have solved the barotropic stability problem for the 1-, 2-, and 3-element cases.

For the y direction we use a spectral decomposition consistent with the boundary condition (12),

$$g_m = \sin[m\pi(y + L)/2L], \\ m = 1, 2, \dots, M. \quad (17)$$

For the double cosine jet the denominator $2L$ is replaced by $4L$. Typically M was either 20 or 40 in our barotropic stability analysis. It is convenient to think of the product $f_j g_m$ as a single basis function h_i , where $i = M(j - 1) + m$. The maximum value of i is therefore $M \times J$, which we denote by N . The Galerkin method involves substituting the expansions of the form (16) into Eqs. (4) and (5), multiplying by each of the basis functions h_i , and integrating over the domain. Since there are N basis functions and two differential equations, one obtains $2N$ linear algebraic equations in the $2N$ unknown coefficients for ϕ and \mathbf{w} .

As discussed by Haltiner and Williams, the Galerkin method leads naturally to energy conservation in equations with quadratic energy invariants. The latter phrase refers to the terms in the expression for the energy of the system. In our problem these are the terms on the left side of Eq. (11), which are quadratic in ϕ and \mathbf{w} . One forms the Galerkin integrals of (4) and (5) as if one were deriving the energy equation (11). This means multiplying (4) and (5) by ρh_i and not simply by h_i before integrating with respect to y and z . With this method the energy equation (11) is satisfied exactly when the basis function expansion (16) is used for ϕ and \mathbf{w} .

In finite element jargon the boundary

condition (6) is a natural boundary condition (e.g., Bathe, 1982). Such boundary conditions either involve derivatives (e.g., $\partial\phi/\partial z$) or cross terms (e.g., both \mathbf{w} and ϕ). To satisfy such conditions one integrates by parts as if forming the energy integrals. The derivatives and cross terms are eliminated from the surface terms by substituting the expressions for the boundary conditions. These terms then appear in the Galerkin equations. In our case the surface term arising from (6) is always zero because it is multiplied by ρ , which vanishes at the planetary surface $z = \pm \sin \lambda$.

The method is much simpler when \bar{u} is constant (or zero). Then the disturbance has the form (15), and the basis function representation is simply

$$\phi = \sum_{j=1}^J \phi_j f_j(z), \quad (18)$$

with a similar expression for \mathbf{w} . It becomes possible to compare the 4-, 8-, and 16-element models in this case. One result of this comparison is that the method does well in satisfying the boundary condition (6) even without the factor of ρ . We find that the ratio \mathbf{w}/ϕ at the surface differs from the desired value $\cot \lambda$ by amounts less than $(J/2)^{-2}$. For the 8-element model ($J/2 = 8$) the error is less than $1/64$. For the 4-element model the error is less than $1/16$. This satisfying of the boundary condition (6) goes beyond what is required for energy conservation, which is taken care of automatically by the fact that $\rho = 0$ at the surface.

The Galerkin representation of two variables ϕ and \mathbf{w} with N basis functions leads to a linear eigenvalue problem of order $2N \times 2N$, namely,

$$\mathbf{B}\mathbf{X} = c\mathbf{A}\mathbf{X}. \quad (19)$$

Here \mathbf{X} is the vector of length $2N$ containing the unknown coefficients ϕ_i and \mathbf{w}_i that appear in the expansions (16) or (18). The $2N \times 2N$ matrices \mathbf{A} and \mathbf{B} contain the integrals of each basis function with every other basis function multiplied by the ap-

appropriate functions $\bar{u}(y)$, $\rho(z, r_0)$, and so on, that appear in (4) and (5). Finally c is the unknown eigenvalue, having the same meaning as in Eqs. (1)–(5).

Equation (19) was solved using IMSL library subroutines INV2F, EIGRF, and EIGZF on a VAX 11/780 computer. These routines give all $2N$ eigenvalues, each with its own eigenvector. Only some of these solutions are physically significant, however. The meaningful solutions look the same regardless of how many basis functions are added to the representation. For J and M sufficiently large they vary smoothly in y and z . And in the barotropic stability problem they are frequently associated with the fastest-growing solution. The other solutions are artifacts of the discrete representation. They vary wildly with respect to y and z ; their eigenvalues change drastically when more elements or more sine functions are added to the representations (16)–(18). And unfortunately, when \bar{u} is not constant they sometimes have finite growth rates. Problems arise particularly when the physically meaningful solutions have zero growth rates. Then the spurious solutions cannot be eliminated on the basis of growth rate alone. They must be examined by varying the resolution (number of basis functions) before any physically meaningful conclusions are drawn.

RESULTS: BAROTROPIC INSTABILITY

Two kinds of problems were investigated: the stability of the cosine jet $\bar{u} = u_0 \cos(\pi y/L)$, and the propagation of waves with $\bar{u} = 0$. In both cases the goal was to extend the results of IP, which are valid only in the limit $k \rightarrow 0$. In that limit ϕ depends only on y and obeys Eqs. (54)–(56) of IP, which are

$$(\bar{u} - c) \frac{d^2\phi}{dy^2} + \left(B - \frac{d^2\bar{u}}{dy^2} \right) \phi = 0, \quad (20)$$

$$B = \frac{2\Omega}{H} \frac{dH}{dr}, \quad H = \int_{-h}^h \rho dz. \quad (21)$$

Here we are using dimensioned variables,

so $h = a_0 \sin \lambda$. A useful formula, valid when ρ approaches zero linearly near the outer surface as in (9), is

$$-B \sin^2 \lambda \rightarrow (3.00)2\Omega/a_0, \quad \lambda \rightarrow 0. \quad (22)$$

In general B , which plays the role of β in the barotropic vorticity equation of meteorology, is negative. This means that disturbances with $k \rightarrow 0$ cannot grow unless $d^2\bar{u}/dy^2$ is more negative than B somewhere in the region.

If the cylindrical flow $\bar{u}(y)$ is projected onto the planetary surface using $dy = -dr$ and $r = a_0 \cos \lambda$, the necessary criterion for instability is

$$\frac{1}{\sin^2 \lambda} \left(B \sin^2 \lambda - \frac{1}{a_0^2} \frac{d^2\bar{u}}{d\lambda^2} \right) > 0. \quad (23)$$

This condition is most likely to be satisfied near the peaks of the eastward jets. Equation (22) gives the value of $B \sin^2 \lambda$ as $\lambda \rightarrow 0$. At $\lambda = 30^\circ$ the value of $B \sin^2 \lambda$ is $(-3.29)\beta$, where $\beta = 2\Omega \cos \lambda/a_0$. At all latitudes $B \sin^2 \lambda$ is between -3β and -4β , according to IP. Figure 1 shows a comparison between the observed curvature $(1/a_0^2)d^2\bar{u}/d\lambda^2$ and $B \sin^2 \lambda$. If barotropic instabilities of the type considered by IP were limiting the curvature of the zonal flow, the two curves should approach each other but not cross.

For the cosine jet (10) the most negative curvature of \bar{u} as a function of y (or r) is $-u_0\pi^2/L^2$. If this were equal to B at latitude $\lambda = 30^\circ$, one would have

$$u_0 r_0 / 2\Omega L^2 = 1.0003, \quad \lambda = 30^\circ. \quad (24)$$

For larger values of $u_0 r_0 / 2\Omega L^2$ the flow would be unstable. We shall call this the Rayleigh criterion, because of the similarity to Rayleigh's analysis for parallel shear flows (e.g., Greenspan, 1968). However, (20)–(24) are applicable only for long-wavelength disturbances ($k \rightarrow 0$).

Figure 2 shows the growth rate contours for $0 \leq kL \leq 3$, where k is the physical wavenumber and L is defined from the profile width in (10). The results are a compos-

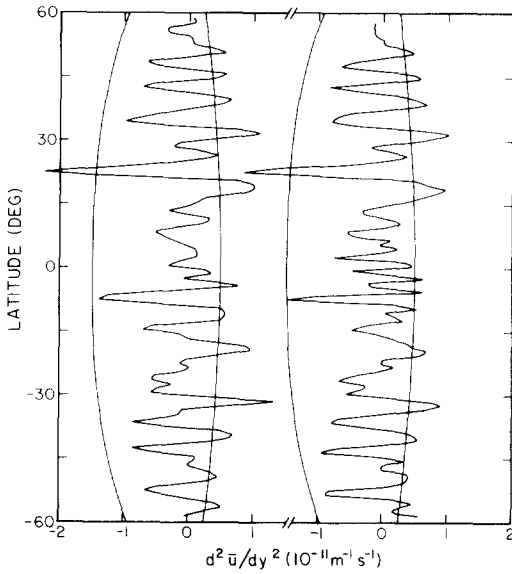


FIG. 1. Curvature or second derivative of Jupiter's zonal velocity profile, after Ingersoll and Pollard (1982). The original data are from Ingersoll *et al.* (1981). Here \bar{u} is the mean eastward wind speed and y is the northward horizontal coordinate (different from y in the text). Voyager 1 data are on the left and Voyager 2 data are on the right. The smooth curve to the right of each profile is β , the planetary vorticity gradient for thin spherical shells. The smooth curve to the left of each profile is $B \sin^2 \lambda$, which is relevant for deep fluid spheres. The observed profiles rarely cross the left curve but often cross the right curve, suggesting that a deep interior flow with the observed curvature might be marginally stable.

ite of 1-, 2-, and 3-element calculations, with 20, 40, and occasionally 80 sine functions in the spectral decomposition. The fact that the zero growth rate contour does not intersect the line $k = 0$ at the Rayleigh criterion is due mostly to the sidewall boundary condition (12). Runs for the double and quadruple cosine jets give results that approach the Rayleigh criterion within 1%.

Figure 2 extends the results of IP upward from the horizontal axis, that is, from $k = 0$. The peak in the growth rate occurs near $kL = 1$, $u_0 r_0 / (2\Omega L^2) = 1.5$. Instability still sets in near $u_0 r_0 / (2\Omega L^2) = 1$ over a range of kL from 0 to 2. There are no growing solutions for $kL > 2$. Nevertheless, Fig. 2 basically confirms IP by indicating that the Rayleigh

criterion (24) based on the theory for $k \rightarrow 0$ provides a good criterion for stability for all disturbance wavenumbers. The phase speed contours (normalized by u_0) indicate that the fastest-growing disturbance tends to travel with that part of the flow where the Rayleigh criterion is marginally satisfied, that is, where $B - d^2 \bar{u} / dy^2$ is close to zero. For values of $u_0 r_0 / (2\Omega L^2)$ close to 1.0 the criterion is satisfied at the peak of the jet ($c_r = 1.0$). For values around 1.5 the criterion is satisfied further down the sides of the jet ($c_r = 0.65$).

Figure 3 gives a representation of the fastest-growing disturbance near $kL = 1.0$, $u_0 r_0 / (2\Omega L^2) = 1.5$. It is an even disturbance in that the streamfunction ϕ and the x and y components of velocity are symmetric about the equator $z = 0$. The northward axial velocity ikw is antisymmetric. This is the only physically meaningful solution that can grow for this value of $u_0 r_0 / (2\Omega L^2)$. We show the results of the 1-element calculation. The 2-element calculation is essen-

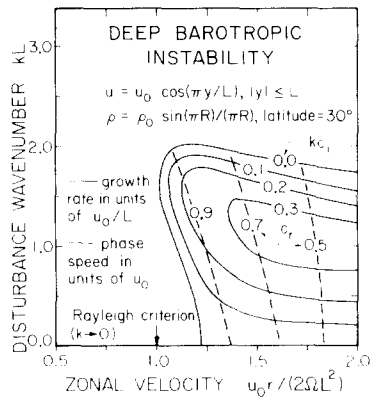


FIG. 2. Growth rates and phase speeds of disturbances on the cosine jet. Here y is distance inward from the cylinder of radius r_0 . The cylinder meets the surface of the sphere at latitude 30° . Density ρ depends on the spherical radius R , with $R = 1$ and $\rho = 0$ at the planet's surface. The eastward wavenumber of the disturbance is k , and the half-width of the jet is L . The arrow labeled Rayleigh criterion indicates the onset of deep barotropic instability when sidewall effects are unimportant and $kL \rightarrow 0$; this criterion was originally derived by Ingersoll and Pollard (1982) for deep spheres.

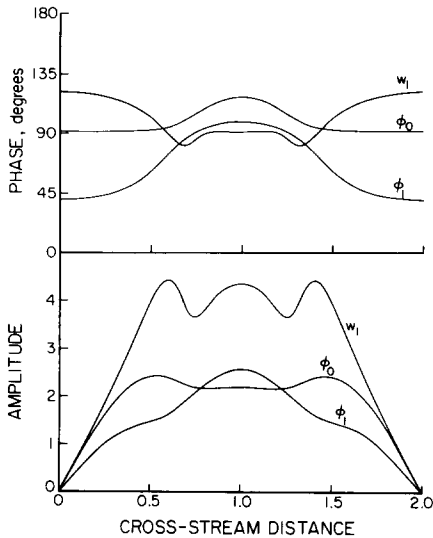


FIG. 3. Complex phase and amplitude of the fastest growing disturbance at $kL = 1$ and $u_0 r_0 / 2\Omega L^2 = 1.5$ (Fig. 2). Here ϕ_1 and ikw_1 are the streamfunction and axial velocity, respectively, at the surface of the planet, and ϕ_0 is the streamfunction in the equatorial plane. Only the relative amplitudes and phases are significant. As $kL \rightarrow 0$ the three phases approach a common curve.

tially the same; the phase speed and growth rate differ by 10^{-3} and 10^{-2} , respectively, between the two calculations. The streamfunction and axial velocity at the surface are ϕ_1 and ikw_1 ; the streamfunction at the equator is ϕ_0 . The zonal velocity profile is a full cosine with maximum eastward velocity in the middle of the figure. Cross stream distance is simply y/L as in (10) with the origin displaced by one unit.

The phases of ϕ_0 and ϕ_1 as functions of distance from the jet center are perhaps the most interesting feature of Fig. 3. The energy equation (14) requires that $\overline{u'v'}$ be positive where $d\bar{u}/dy$ is negative and vice versa. An alternate expression for $\overline{u'v'}$, which appears in (11), is $-(k/2)\text{Im}(\phi^* \partial \phi / \partial y)$. This is equal to $-(k/2)|\phi|^2 \partial p / \partial y$, where $p(\phi) = \tan^{-1}(\phi_i / \phi_r)$ is the phase of the complex amplitude of the streamfunction defined in (1) and (2). Thus a growing disturbance must have $\partial p / \partial y$ positive where $\partial \bar{u} / \partial y$ is positive and vice versa. This requirement is confirmed in Fig. 3, which

shows that the phases of ϕ_0 and ϕ_1 both have maxima near the jet center, where \bar{u} has its maximum. The fact that the phase change is of order 45° in a distance L means that the negative correlation between $\overline{u'v'}$ and $d\bar{u}/dy$ would be clearly observable if these were the dominant eddies. As stated earlier a positive correlation is observed in the visible atmosphere (Ingersoll *et al.*, 1981).

These disturbances have a substantial amount of energy associated with their axial motion. The three terms on the left side of (11) are associated with the x , y , z components of velocity, respectively, and they are all of the same order of magnitude. Despite this large axial velocity, the motion is geostrophic in the xy plane. The last fact follows from the smallness of L/a_0 and the fact that the motion is quasi-columnar.

The physically significant modes, which vary smoothly in y , are insensitive to the number of terms in the basis function expansion. As already stated, the eigenvalue c varies by less than 1% at $kL = 1$, $u_0 r_0 / (2\Omega L^2) = 1.5$ when the 1-element solution is compared to the 2-element solution. Similar changes were noted in comparing the 20-term and the 40-term sinusoidal expansions in y . However for larger values of kL (e.g., $kL \geq 3$), the spurious modes have substantial growth rates ($kc_i \geq 0.3$). These modes oscillate rapidly in y , and their growth rates decrease as more terms are taken in the sinusoidal expansion. Yet they would cause trouble in a nonlinear time-dependent calculation that was designed to follow the physically significant modes as they grow to finite amplitude.

RESULTS: INERTIAL OSCILLATIONS

The other application of these methods is to normal mode oscillations where $\bar{u} = 0$. Since rotation provides the restoring force, they will be called inertial oscillations (e.g., Greenspan, 1968). Other authors (Hide, 1966; Glatzmaier and Gilman, 1981) have discussed these phenomena in other contexts. Ours is perhaps the first application

to Jupiter and Saturn. As shown earlier, the disturbance has the form (15). For comparison with observations it is useful to project this variation onto the surface of the sphere and choose L^{-1} to be the projected wavenumber. This is accomplished by letting $k_e = (1/L)\cos\theta$ be the eastward wavenumber as seen at the surface and $k_n = (1/L)\sin\theta$ be the corresponding northward wavenumber, with $k_e = k$ and $k_n = n \sin\lambda$. The last step follows because the rapid variation in r is spread out when projected onto the surface. The phase speed c_p of a wave as it moves over the surface of the sphere at angle θ to the eastward direction is then

$$c_p = ck_e(k_e^2 + k_n^2)^{-1/2} = c \cos\theta, \quad (25)$$

where c is the quantity appearing in Eqs. (1)–(3).

For fixed L the phase speed c_p is a function only of the direction of propagation. A vector of length c_p at angle θ to the x axis traces out a curve that defines the wave. For example, a Rossby wave for a fluid in a thin spherical shell has

$$c_p = c \cos\theta = \frac{-\beta \cos\theta}{k_e^2 + k_n^2} = -\beta L^2 \cos\theta, \quad (26)$$

where $\beta = (2\Omega/r_0)\cos^2\lambda$. The propagation speed c_p cannot be negative, so the Rossby wave phase speed has no eastward component—it plots as a circle of diameter $2\Omega L^2 \cos^2\lambda/r_0$ centered half a diameter to the west of the origin.

As another example, the analysis of IP gives phase speeds in the limit $k/n \rightarrow 0$, i.e., $\cos\theta \rightarrow 0$. For $\bar{u} = 0$, Eq. (20) gives $c = -B/n^2$. This relation combined with (25) yields

$$c_p = -(B \sin^2\lambda/\beta)\beta L^2 \cos\theta, \quad (27)$$

since $n^2 = 1/(L \sin\lambda)^2$ in this limit. As stated in connection with Eq. (23), $-B \sin^2\lambda$ is three to four times β and is equal to $(3.29)\beta$ at $\lambda = 30^\circ$. So at latitude 30° we have, for $|\cos\theta| \ll 1$,

$$c_p = (3.29)\beta L^2 \cos\theta. \quad (28)$$

This looks like the Rossby wave circle (26), except it is 3.29 times larger and its center lies half a diameter to the *east* of the origin. However, the analysis of IP defines only the start of the curve—the vertical part that lies close to the y axis. This part describes northward and southward propagating waves, and also eastward and westward propagating waves that are trapped within latitudinal limits that are small compared to the east–west wavelength. The analyses by Hide (1966) and by Glatzmaier and Gilman (1981) were also subject to these restrictions.

The methods developed in this paper allow us to complete the curve for all directions of propagation (values of θ). We can also investigate higher modes, those for which the phase of the oscillation changes with respect to z . We define the M th mode as an oscillation with M nodes (zero crossings—not to be confused with finite element nodes) between $z = -\sin\lambda$ and $z = \sin\lambda$. IP's results are for the 0th mode (in-phase oscillations at all z).

Figure 4 shows the curves at latitude 30° , using the 8-element model. The results differ from the 16-element model by less than 0.01%. The speeds are shown scaled by $V \cdot 2\Omega L^2/r_0$, where V is the unit indicated with each curve. Mode 0 propagates eastward with a maximum phase speed of $(8.363)2\Omega L^2/r_0$. This mode does not propagate westward. Mode 1, for which the oscillations in the northern and southern hemispheres are 180° out of phase, propagates eastward with a maximum phase speed of $(11.502)2\Omega L^2/r_0$. Its maximum westward speed is $(0.943)2\Omega L^2/r_0$. Higher modes have higher speeds. The Rossby wave, which is not an internal mode, is shown for reference only. Its maximum westward speed is $(0.750)2\Omega L^2/r_0$.

According to Fig. 4, the complete curve is not a circle; the phase speed is strongly peaked in the direction of eastward propagation. This peaking increases as the latitude decreases. Table I shows the eastward phase speed ($\cos\theta = 1$) for the lowest even

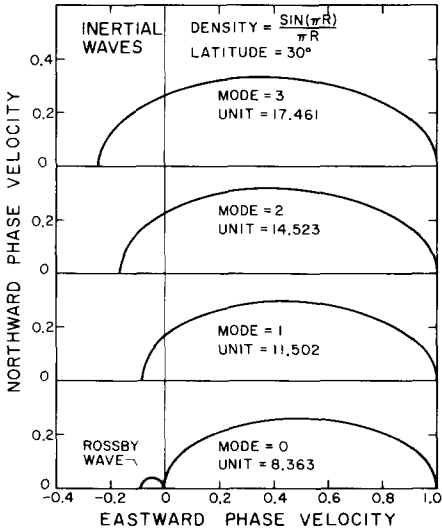


FIG. 4. Propagation diagram for deep inertial waves projected onto the surface of the sphere at latitude 30°. The length of the vector from the origin to the curve represents the phase speed scaled by $V2\Omega L^2/r_0$, where V is the unit indicated, and $2\pi L$ is the wavelength projected onto the surface. The lowest four axial modes are shown. The Rossby wave curve is for thin spherical shells, and is shown for reference purposes. Density is assumed to vary as $\sin(\pi R)/(\pi R)$ as in Fig. 2.

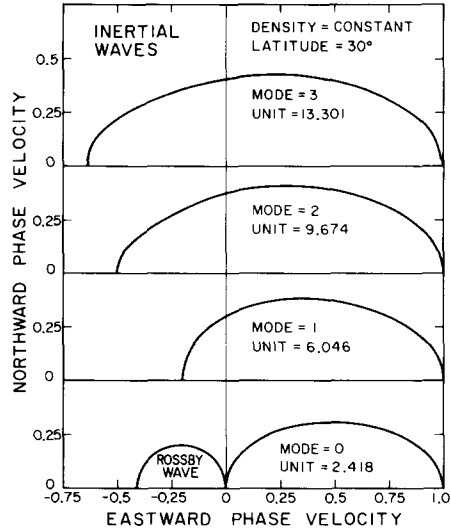


FIG. 5. As in Fig. 4 but for constant density.

mode (mode 0) and the eastward and westward phase speeds ($\cos \theta = \pm 1$) for the lowest odd mode (mode 1). These results are for pure east-west propagation, waves with no variation in y . Below we consider waves that are trapped in y , i.e., waves whose north-south wavenumber n is much larger than the east-west wavenumber k al-

though the waves propagate only in the east-west direction.

Figures 5 and 6 show the results for a constant density sphere. According to (21), H is then $2a_0 \sin \lambda$, and $-B \sin^2 \lambda$ is $(2\Omega/r_0)\cos^2 \lambda$, which is exactly equal to β . Thus, the behavior of the phase speed (27) for $|\cos \theta| \ll 1$ is exactly the same as for a thin atmosphere (26) but with β replaced by $-\beta$. Figure 5 shows that the complete phase

TABLE I

MAXIMUM PHASE SPEEDS (POSITIVE EASTWARD) IN UNITS OF $2\Omega L^2/r_0$

Latitude (deg)	Internal modes			Rossby wave
	0	1	1	
15	32.54	39.56	-0.986	-0.933
30	8.363	11.502	-0.943	-0.750
45	3.271	5.072	-0.862	-0.500
60	1.232	2.311	-0.719	-0.250
75	0.2861	0.8335	-0.464	-0.067

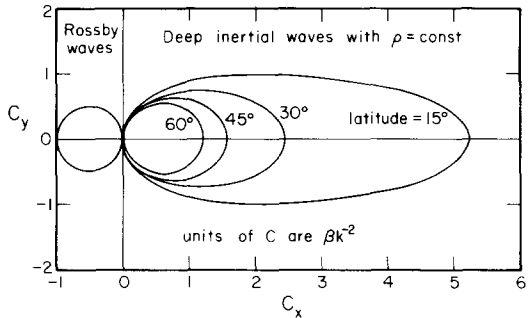


FIG. 6. As in Fig. 4 but for constant density and scaling appropriate to Rossby waves. The phase speed is scaled by βk^{-2} or $2\Omega L^2 \cos^2 \lambda/r_0$, so Rossby waves plot as a circle of unit diameter for all latitudes λ . The lowest mode (mode 0) is shown at latitudes of 15°, 30°, 45°, and 60°. The pronounced peak associated with pure eastward propagation increases as the latitude decreases.

speed curve is elongated in the direction $\cos \theta = 1$, but less so than when density decreases outward (Fig. 4). Figure 6 shows the latitude variation of the mode 0 curve, and illustrates the fact that the degree of elongation for $\cos \theta = 1$ increases toward the equator.

We now compare the phase speeds of Fig. 4 and Table I to the 100 m/sec zonal velocities that are typical of Jupiter and Saturn. The rationale is that some of the observed phenomena might be related to deep inertial waves. We do not suggest a mechanism; our aim is merely to see which of the quasi-columnar inertial oscillations are in the right ranges of wavelengths and phase speeds.

We treat the latitudinal bands as waveguides although the mechanism of trapping is unclear. Projected onto the equatorial plane the y variation of the zonal velocity profile is roughly sinusoidal, with a wavelength of order 12,000 km (e.g., IP Figs. 3–5). At middle latitudes where B can be regarded as constant, the trapped wave has the form

$$f(z) \cos(ny) \exp[ik(x - ct)], \quad (29)$$

with $L = 1/n$ of order 12,000/2 π km, or 2000 km. Equation (29) is equivalent to (15), but it now describes an eastward or westward propagating wave ($c > 0$ or $c < 0$) with a standing wave (trapped) structure in y . Three cases are considered: long waves trapped in a narrow midlatitude band ($k \ll n$), short waves trapped in a relatively wide midlatitude band ($k \gg n$), and long waves trapped in a narrow band on the equator.

For $k \ll n$ the analysis of IP is applicable. Equation (20) gives $c = -B/n^2$, where $-B \sin^2 \lambda$ is of order 3β , or $(6\Omega/a_0) \cos \lambda$ according to (22). Since c is independent of k the waves are nondispersive. For Jupiter with $n = 1/(2000 \text{ km})$, we have

$$c \approx \frac{6\Omega \cos \lambda}{a_0 n^2 \sin^2 \lambda} \approx \left(60 \frac{\text{m}}{\text{sec}}\right) \frac{\cos \lambda}{\sin^2 \lambda}. \quad (30)$$

This is a high speed. At latitudes of 45°, 30°, and 15°, the eastward speeds are 85, 208,

and 865 m/sec, respectively, according to the above formula. Shorter waves move more slowly, as do waves trapped on the equator.

For $k \gg n$ the results of Table I are applicable. Now the east–west wavenumber determines the scale, and L is $1/k$. For $L = 1000 \text{ km}$ at latitudes of 45°, 30°, and 15°, the eastward speeds are 23, 48, and 166 m/sec, respectively, for mode 0 oscillations. For shorter waves the propagation speeds fall as L^2 . The waves are dispersive; the dependence on L is similar to that for Rossby waves.

For long waves trapped on the equator Eq. (20) is applicable, but B cannot be regarded as constant. Instead from (22) we have

$$-B \approx 6\Omega/(a_0 \sin^2 \lambda) \approx 3\Omega/y, \quad (31)$$

where y is radial distance inward from the surface of the planet at the equator:

$$y = a_0 - a_0 \cos \lambda \approx (a_0/2) \sin^2 \lambda. \quad (32)$$

With $\bar{u} = 0$, Eq. (20) becomes

$$\frac{d^2 \phi}{dy^2} + \frac{3\Omega}{cy} \phi = 0, \quad (33)$$

the solution of which is a Bessel function (e.g., Abramowitz and Stegun, 1965, formula 9.1.50):

$$\phi(y) = y^{1/2} Z_1(s), \quad s = 2(3y\Omega/|c|)^{1/2}, \quad (34)$$

where Z_1 is J_1 or Y_1 for $c > 0$, and is I_1 or K_1 for $c < 0$. Of these four choices only J_1 is relevant to equatorial waves. For this solution ϕ oscillates regularly in y and vanishes at $y = 0$. Since $ik\phi$ is the inward radial velocity, the condition $\phi = 0$ at $y = 0$ corresponds to having vertical velocity vanish at the planet's surface, as it should. The Y_1 and K_1 solutions do not vanish at $y = 0$ and have logarithmically singular derivatives. The I_1 solution does vanish at $y = 0$, but it grows exponentially in y . The J_1 solution propagates to the east and has its first zero at $s = 3.8317$.

It is tempting to associate these long-wavelength, eastward propagating waves

with the equatorial plumes that were seen in the latitude band $0 \leq \lambda \leq 9^\circ$ at the time of Voyager (Smith *et al.*, 1979, Fig. 1). Setting $s = 3.8317$ at $\lambda = 9^\circ$ gives

$$c = \frac{3}{2} \left(\frac{2}{3.8317} \right)^2 \Omega a_0 \sin^2 \lambda = 126 \text{ m/sec.} \quad (35)$$

This is only slightly greater than the eastward velocity of the plumes, but the agreement is fortuitous. First, we have not identified a trapping mechanism, and the value of λ at which to apply Eq. (35) is uncertain by a factor of 2 or more. Second, any trapping mechanism probably involves the zonal velocity profile $\bar{u}(y)$ which we have left out of this analysis. Third, Eq. (20) describes a mode 0 solution, but there is no evidence that the northern and southern hemispheres were oscillating in phase at the time of Voyager. Fourth, we have not identified an excitation mechanism, and therefore have no basis for associating the motion of the plumes with the propagation of an equatorial wave.

DISCUSSION

The theoretical model allows us to study a class of motions that could occur in a rotating fluid planet. The physical system is a simple one. The fluid is inviscid and adiabatic, and density is allowed to vary from its value at the center to the value zero at the surface. Other studies have emphasized the effects of viscosity, thermal stratification, heat sources, energy dissipation, and other processes. Given our ignorance about the interiors of the giant planets, many approaches are possible. A goal of these studies should be to define the relationships between potentially observable quantities so that observations may be used to limit the theoretical possibilities. Another goal is simply to learn about rotating fluid planets by systematically studying idealized systems and not worrying about realism. Both goals are consistent with this paper.

With these caveats in mind, we briefly

summarize the results of this paper and their relation to observations. First, the limiting condition for stability of a deep zonal flow is similar to that found by IP, who considered only disturbances with small zonal wavenumber. As shown by IP, Jupiter's and Saturn's zonal velocity profiles are marginally stable according to this criterion. On the other hand, the data refer to the cloud tops and do not define the curvature of the profile with high accuracy. Also the theory is limited by the assumptions that the interior is inviscid and adiabatic. And from the correlation between $\overline{u'v'}$ and $d\bar{u}/dy$, it is clear that the eddies observed in the cloud zone are not the same as the fastest-growing eddies found in the theory. The latter extract kinetic energy from the shear flow; the former put energy in. Processes that were not considered in this model clearly are active in Jupiter's and Saturn's cloud zone.

The results of comparing the theory of deep inertial oscillations with observations of waves in the atmosphere are equally ambiguous. Many structures look like waves confined within a band of latitude. Yet the confinement mechanism and the wave excitation mechanism are beyond the scope of this theory. For some choices of latitudinal bandwidth and eastward wavelength, the eastward propagation speeds of the theory are in the general range of observed velocities. This fact encourages us in our theoretical studies, but it does not prove that the observed waves are related to deep inertial oscillations.

APPENDIX

The coordinate system is complicated because we use both spherical and cylindrical coordinates, and we employ two length scales to describe variations perpendicular to the axis of rotation. The cylindrical radial coordinate is r , and r_0 is a reference value equal to the radius of the cylinder at the zonal jet maximum. The axial coordinate is z , which measures distance above the equatorial plane. The spherical radial

coordinate is R , so that $R = (r^2 + z^2)^{1/2}$. The value of R at the surface of the planet is a_0 , the planetary radius. The latitude $\cos^{-1}(r_0/a_0)$ where the reference cylinder meets the planetary surface is λ . The height h of the cylinder is $a_0 \sin \lambda$. Flow quantities such as velocity and streamfunction are assumed to vary with respect to r on a short length scale L . For these variations we use the inward radial coordinate $y = r_0 - r$. Density is assumed to vary only on the long length scale a_0 , and we use the coordinates r and z . Distance to the east is denoted by x . The flow quantities are assumed to vary with respect to x on the short length scale L , and are assumed to vary with respect to z on the long length scale a_0 . Thus x , y , z define the Cartesian coordinate system used in this paper.

ACKNOWLEDGMENTS

This research was started while one of us (RLM) held a Summer Undergraduate Research Fellowship (SURF Program) at Caltech. Further support was provided through the Planetary Atmospheres Program of NASA.

REFERENCES

- ABRAMOWITZ, M., AND I. A. STEGUN (1965). *Handbook of Mathematical Functions*. Dover, New York.
- BATHE, K.-J. (1982). *Finite Element Procedures in Engineering Analysis*. Prentice-Hall, Englewood Cliffs, N.J.
- GLATZMAIER, G. A., AND P. A. GILMAN (1981). Compressible convection in a rotating spherical shell. III. Analytic model for compressible vorticity waves. *Astrophys. J. Suppl. Ser.* **45**, 381–388.
- GREENSPAN, H. P. (1968). *The Theory of Rotating Fluids*. Cambridge Univ. Press, Cambridge.
- HALTNER, G. J., AND R. T. WILLIAMS (1980). *Numerical Prediction and Dynamic Meteorology, 2nd ed.* Wiley, New York.
- HIDE, R. (1966). Free hydromagnetic oscillations of the Earth's core and the theory of the geomagnetic secular variation. *Philos. Trans. R. Soc. London, Series A* **259**, 615–650.
- HOLTON, J. R. (1979). *An Introduction to Dynamic Meteorology, 2nd ed.* Academic Press, New York.
- INGERSOLL, A. P., R. F. BEEBE, B. J. CONRATH, AND G. E. HUNT (1984). Structure and dynamics of Saturn's atmosphere. In *Saturn* (T. Gehrels and M. S. Matthews, Eds.), pp. 195–238. Univ. of Arizona Press, Tucson.
- INGERSOLL, A. P., R. F. BEEBE, J. L. MITCHELL, G. W. GARNEAU, G. M. YAGI, AND J. P. MULLER (1981). Interaction of eddies and mean zonal flow on Jupiter as inferred from Voyager 1 and 2 images. *J. Geophys. Res.* **86**, 8733–8743.
- INGERSOLL, A. P., AND P. G. CUONG (1981). Numerical model of long-lived Jovian vortices. *J. Atmos. Sci.* **38**, 2067–2076.
- INGERSOLL, A. P., AND D. POLLARD (1982). Motion in the interiors and atmospheres of Jupiter and Saturn: Scale analysis, anelastic equations, barotropic stability criterion. *Icarus* **52**, 62–80.
- MAC LOW, M.-M., AND A. P. INGERSOLL (1985). Merging of vortices in the atmosphere of Jupiter: An analysis of Voyager images. *Icarus* **65**, 353–369.
- OGURA, Y., AND N. A. PHILLIPS (1962). Scale analysis of deep and shallow convection in the atmosphere. *J. Atmos. Sci.* **19**, 173–179.
- POINCARÉ, H. (1910). Sur la precession des corps déformables. *Bull. Astron.* **27**, 321–356.
- SMITH, B. A., L. SODERBLOM, R. BATSON, P. BRIDGES, J. INGE, H. MASURSKY, E. SHOEMAKER, R. BEEBE, J. BOYCE, G. BRIGGS, A. BUNKER, S. A. COLLINS, C. J. HANSEN, T. V. JOHNSON, J. L. MITCHELL, R. J. TERRILE, A. F. COOK II, J. CUZZI, J. B. POLLACK, G. E. DANIELSON, A. P. INGERSOLL, M. E. DAVIES, G. E. HUNT, D. MORRISON, T. OWEN, C. SAGAN, J. VEVERKA, R. STROM, AND V. E. SUOMI (1982). A new look at the Saturn system: The Voyager 2 images. *Science* (Washington, D.C.) **215**, 504–537.
- SMITH, B. A., L. A. SODERBLOM, R. BEEBE, J. BOYCE, G. BRIGGS, M. CARR, S. A. COLLINS, A. F. COOK, G. E. DANIELSON, M. E. DAVIES, G. E. HUNT, A. INGERSOLL, T. V. JOHNSON, H. MASURSKY, M. MCCAULEY, D. MORRISON, T. OWEN, C. SAGAN, E. M. SHOEMAKER, R. STROM, V. E. SUOMI, AND J. VEVERKA (1979). The Galilean satellites and Jupiter: Voyager 2 imaging science results. *Science* (Washington, D.C.) **206**, 927–950.